A New Contactless Fault Diagnosis Approach for Pantograph-Catenary System Using Pattern Recognition and Image Processing Methods

İlhan AYDIN, Mehmet KARAKÖSE, Erhan AKIN
Computer Engineering Department, Firat University, 23119, Elazig, Turkey
iaydin@firat.edu.tr, mkarakose@firat.edu.tr, eakin@firat.edu.tr

[1]***Abstract*—Comfort and safety of railway transport has become more important as train speeds continue to increase. In electrified railways, the electrical current of the train is produced by the sliding contact between the pantograph and catenary. The quality of the current depends on the reliability of contact between the pantograph and catenary. So, pantograph inspection is very important task in electrified railways and it is periodically made for preventing dangerous situations. This inspection is operated manually by taking the pantograph to the service for visual anomalies. However, this monitoring is impractical because of time consuming and slowness, as locomotive remains disabled. An innovative method based on image processing and pattern recognition is proposed in this paper for online monitoring of the catenary-pantograph interaction. The images are acquired from a digital line-scan camera. Data are simultaneously processed according to edge detection and Hough transform, and then the obtained features are provided to a D-Markov based state machine, and the pantograph related faults, such as overheating of the pantograph strip, bursts of arcing, and irregular positioning of the contact line are diagnosed. The proposed method is verified by real faulty and healthy pantograph videos.**

***Index Terms*—Pantograph, catenary, arcing faults, edge detection, Hough transform, fault diagnosis, railways.**

I. INTRODUCTION

In electrified railways, the safe movement of the train is based on the quality of current collection, resulting from sliding contact between a pantograph and an overhead contact wire. A pantograph is the most utilized component for the transmission of electric power from the overhead wire to a locomotive [1]. Any interruption in the contact may damage the overhead line and the pantograph. Poor contact may cause arcing and wearing of the pantograph strips and contact wire. With the development of high-speed electric trains, the demand for safety in railway transport has become increasingly more important. When a high-speed train enters to a tunnel, the oscillation of the contact wire increases, and the pantograph head cannot maintain contact. Pantographs must maintain sufficient contact under different train speeds to ensure the transfer of power without problems [2]. Derailment accidents are prevented by railroad maintenance planning, based on the use of early rail and road anomaly detection technologies.

The pantograph and overhead wire are fundamental components for the collection of current signals in electric trains. The wear between the pantograph and overhead wire results in catastrophic faults. Pantograph arcing is one of the most commonly observed faults in electrified railway systems. Arcing generally occurs at higher speeds, under increased load, and in cold weather conditions [3]. In most cases, a sliding contact occurs between the pantograph and catenary system. A pantograph draws a lateral zigzag pattern on the overhead wire [4]. However, the overhead wire applies more contact to some locations of the pantograph as a result of faulty conditions. Under normal conditions, a moisture layer exists between the contact surface and pantograph. This moisture layer often becomes frozen during winter, leading to increased difficulty in maintaining the sliding contact between two components. Pantograph arcing faults occur because of following reasons [5], including

- Incorrect static contact force,
- Excess friction,
- Incorrectly set aerodynamics,
- Worn components, and
- Poor geometric adjustment.

All railway companies must prepare a maintenance schedule. The most frequently used method consists of periodic inspections of the catenary line and pantograph [6]. This method is expensive, because it requires the line to be temporarily out of service during the inspection. Hence, the inspection activities are performed at night. Another disadvantage associated with this approach is that the inspection cannot be performed over the entire line. Additionally, the locomotives must be maintained in service for pantograph inspection. This method also is undesirable because it causes a loss of service time and increases costs [7]. Therefore, new monitoring equipment and technology have been developed for high-speed operations. Computer based modeling and analysis of critical components of railway system is a cost-effective, safe, and efficient solution [8].

Mechanical sensor-based rail and road measurement and inspection techniques have been used in the railway industry [9-10]. The contact force between the pantograph and catenary system is monitored using fiber strain sensors. Static and dynamic strains are detected by the developed system. With the latest technological developments, contactless measurement techniques are being used in railway measurement systems. Arcing between the pantograph and contact wire has been detected using phototube sensors [11]. These sensors are physically placed on the front and back ends of the pantograph. The arcing

This work was supported by TUBITAK under Grant TUBITAK 112E067.

Digital Object Identifier 10.4316/AECE.2014.03010

conditions are detected by using ultraviolet emissions. A wavelet-based multi-resolution analysis was applied to the traction current measurement to determine the quality of the collected current [6]. The proposed method can reveal both the welding effect and singular arcing events. The position of a pantograph in a railway system has been tracked by a computer vision system [12]. The proposed method estimates the height of the pantograph. This knowledge is used to determine the position of the contact wire. First, the edge of the pantograph image is extracted, and a structural model of the tracked object is obtained. Pantograph arcing was experimentally inspected in a DC railway system [13]. An experimental setup was established to obtain the current and voltage waveforms. The pantograph and overhead wire system were analyzed using an infrared camera [14]. This analysis was used to detect overheating of the pantograph strip, bursts of arcing, and irregular positioning of the contact line. To obtain efficient wear measurements of the contact wire, a new multi-camera-based optical inspection system was proposed [15]. Different cameras were mounted at different positions on the roof of the vehicle, and the overhead contact was visually inspected from various angles. Abrasion on the pantograph slide was detected using an edge detection algorithm [16-17]. A discrete wavelet and Hough transform-based method was applied to images of pantograph sliding, and the abrasion related features were extracted [18]. Five kinds of edge detection algorithms were evaluated for the examination of pantograph slipping images [19]. The results show that the canny edge detection algorithm gives better results than the other algorithms. Image processing-based methods were proposed for monitoring the contact performance [18, 20]. In recent years, the contactless monitoring of railway systems have attracted the attention of researchers. However, the developed system is suitable for laboratory applications. The real-time monitoring of arcing remains a challenging problem, because it distorts the regular waveform of the supply. The arcing generates transients, and these transients affect the railway system, including the track circuits, supply transformers, vehicle transformers, and other locomotives.

This paper presents a new approach for monitoring the contact between pantograph and catenary system. The paper contributes a new methodology that combines image processing with pattern recognition and is able to perform a reliable online assessment of the contact wire condition in an electrified railway system. The proposed method comprises the position detection of contact wire and the analysis of this position by using D-Markov based state machine. The images are acquired for the surface of pantograph-catenary system and canny method is applied to detect edges. The upper side of the pantograph is detected by applying Hough transform to edge image. This knowledge is used to determine the search region of the contact wire. After the position of contact wire is obtained as a signal, D-Markov-based state machine is applied to the extracted signal, and the contact related disorders are detected.

The rest of the paper is organized as follows. Section II explains the fundamental overhead components of the electrified railway system. The sliding movement of the contact wire and its structure also are given in Section II. Section III describes the implementation and algorithmic details of the proposed methodology. Section IV provides the experimental results of the proposed system for healthy and faulty pantographs. The conclusions are given in Section V.

II. Sliding Contact Between the Pantograph and Catenary System

The contact between the pantograph and overhead wire, which is established on the roof of an electric train, allows the current to be collected from the overhead feeding conductor. The contact wire takes the electricity from the feeder stations, which are connected at regular intervals. The catenary and pantograph system is depicted in Fig. 1.

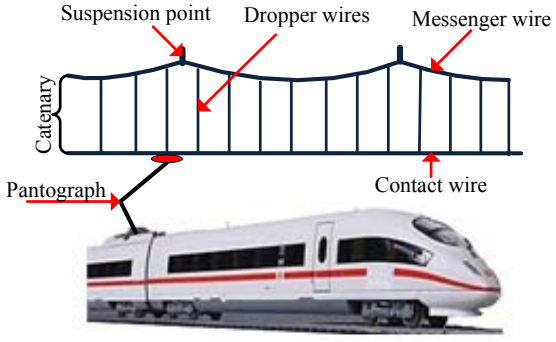

Figure 1. Catenary system and pantograph in an electric train

In Fig. 1, the contact wire is connected to the messenger wire via dropper wires. Several pantograph designs have been developed for use in electrified railway systems. Even so, their contact interfaces are very similar. The upper part of a pantograph generally contains one or more rectangular bars. The most frequently used pantograph types are shown in Fig. 2.

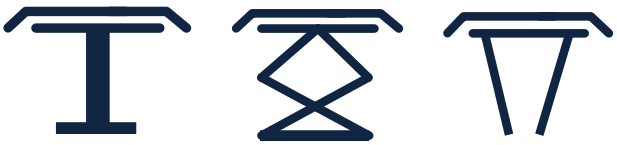

(a) (b) (c)

Figure 2. Designs of pantographs (a) Pantograph of VL-80 (b) Pantograph of Chs-200 (c) Pantograph of TGV

The first pantograph type, which is given in Fig. 2 (a), is a single armed pantograph. This design is widely used on multiple units as well as in several 25 kV AC locomotives. The cross-arm type pantograph was fitted to the recent class 86 locomotives and was fitted standardly for all class 87 locomotives, as depicted in Fig. 2 (b). The most recent pantograph design is the BR/Brecknell pantograph, developed in 1970. This design was agreed upon as the standard for high-speed locomotives by railway manufacturers. This design was first employed on class 87 engines.

Achieving a good balance between the pantograph and contact line depends on the quality of the current collectors and the lifetime of the contact wire. The continuity of the contact is important to ensure better electrical performance. The contact can be maintained by increasing the up-lifting force. However, this increases the resonance of the overhead

wire, which causes the loss of contact and wearing of the contact wire [19]. When the weather conditions change, the contact wire may be upraised or stretched. These two conditions may cause the loss of contact after the points of attachment and they are depicted in Figs. 3 (a) and (b), respectively. When contact has been lost or a gap has occurred, the train power becomes interrupted. The loss of contact also causes arcing between the contact wire and pantograph. For high-speed trains, current collection is based on good contact performance. On a straight path, the contact wire moves slightly to the left and then to the right corner of the pantograph. The border of the movement of the contact wire on the pantograph and its zigzag motion are depicted in Figs. 3 (c) and (d), respectively.

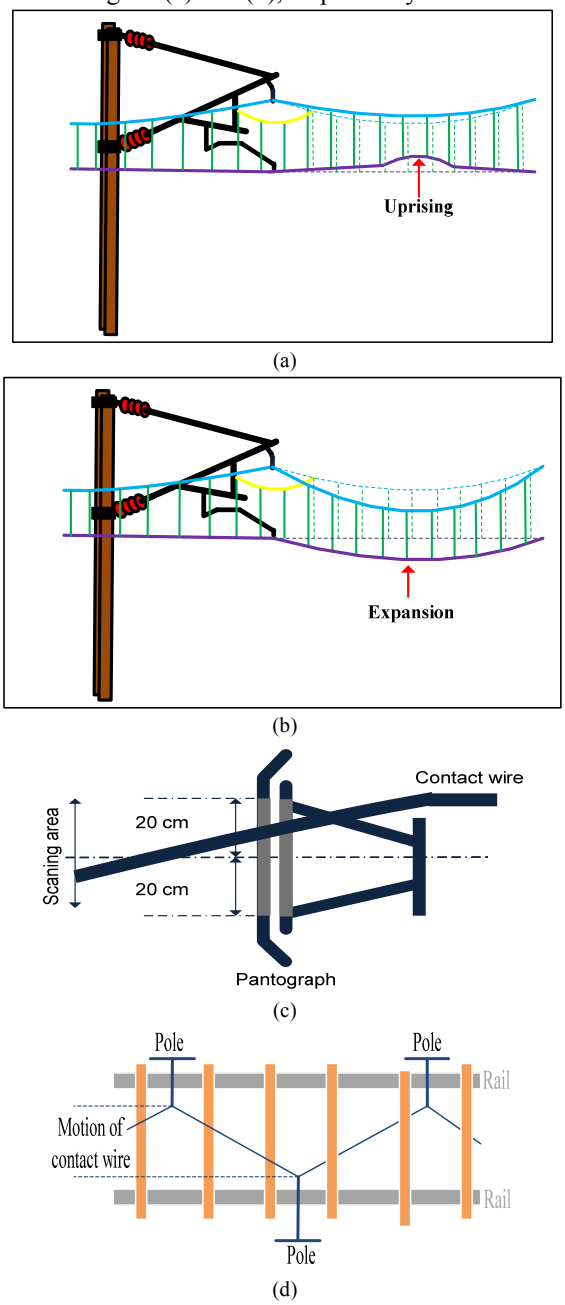

Figure 3. Dynamic behavior of contact wire (a)Uprising of contact wire (b)Expansion of contact wire (c) Sliding view between contact wire and pantograph (d) Motion of contact wire on railway

In Fig. 3, the contact wire applies an impression to different points of the pantograph. Such a system extends the lifetime of the pantograph. The sliding contact between the pantograph and overhead wire consists of three layers. These layers are copper wire, a layer of carbon and oxide, and a thin film of water [21].

The conduction mechanism is realized using the thin film of water. The gap between the two electrodes should be maintained. However, the thin film of water can become frozen during winter, and the sliding contact may stretch [15].

III. The Proposed Method for Contactless Fault Diagnosis in The Pantograph-Catenary System

To monitor automatically the contact wire, the images taken from a camera are used. The main task is to detect the contact points between pantograph and catenary system and to use this information for anomaly detection. Canny algorithm is applied to the current frame in order to extract the edges of the objects in the image. The upper side of the pantograph is obtained by using Hough transform. Edge points are converted to Hough parameter space (r, θ) where parameter r and θ show the intercept and slope of the line, respectively. The contact wire position of each frame is determined from the extracted edge images. The contact point changes in each frame because of contact wire draws zigzag over the pantograph. The position of the contact wire in each frame are obtained and saved as signal, and then the anomalies in this signal are detected using the D-Markov based pattern recognition method. Therefore, the monitoring process is automated. A block diagram of the proposed method is given in Fig. 4.

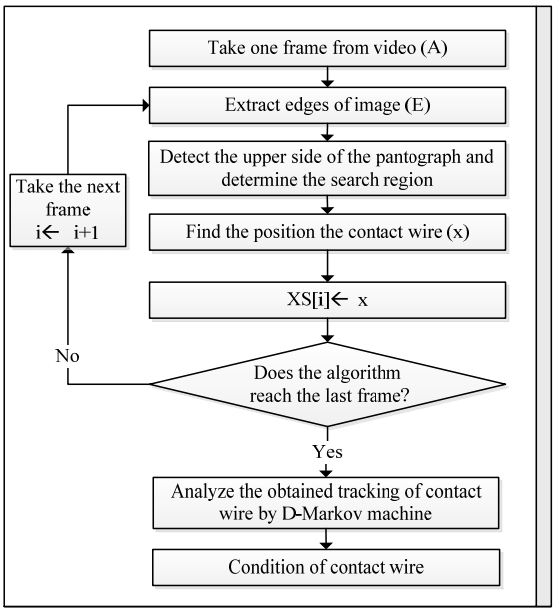

Figure 4. The block diagram of the proposed method

In Fig. 4, the first step is to extract the edge of each frame from the video. The upper side of the pantograph is found, and the search region for the contact wire is determined. Afterwards, the position of the contact wire is detected and added to the array XS. When all frames have been read, the algorithm produces the position array of the x-axis.

A. The Position Detection of the Contact Wire

The first step in the algorithm is to apply the canny algorithm to each frame of the pantograph's video. Each

frame of video is filtered to remove the noise and to establish clearly the image edge. For this purpose, a filter is applied to each frame before applying the canny edge detection algorithm. The edges in an image are defined as the pixels at which the brightness values change suddenly. Edges characterize boundaries, and therefore, they are an important topic in the image processing [22]. An edge detection algorithm generally consists of three steps, including filtering, derivation, and edge detection. In the filtering stage, the image is filtered to remove the noise. In the derivation stage, the edge areas in the image are brightened via density change in the edge area. In the last stage, the edges of the image are determined. The Canny algorithm is known as an optimal edge detection algorithm [23]. After the edge image has been obtained, the position of the contact wire will be detected. The algorithm takes a binary image as an input, which is the edge image produced by the canny edge detection algorithm. The algorithm produces an array of horizontal positions that describe the position of the contact wire throughout all frames. The contact wire of each frame also may move vertically. However, this displacement is rather small in comparison to that of the vertical direction. The position of a contact wire is related to the upper side of the pantograph. Hence, the top position of the pantograph should be detected. The region of the contact wire is determined via Hough transform. This transform is a popular algorithm for detecting the straight lines in an image. It is not affected by gaps in the curves or noise. For a given set of edge points, the data can be explained by finding the lines. The Hough transform is derived from the Radon transform, which is used to identify the collinear lines in an image [24]. First, the Hough transform was used to identify the straight lines in a three-dimensional image. It has been extended to fit regular shapes, such as circles, squares, and ellipses [25]. The Hough transform converts a pixel image into a new space, denoted as the Hough or parameter space. After the line to be searched is determined, each pixel in the image edge votes for this line. The simplest form of the Hough transform is given for detecting straight lines. The straight line can be expressed as

$$y = mx + n \tag{1}$$

where the equation has two parameters for the description of any straight line. These parameters are the slope m and intercept b, respectively. The straight line can be represented as a point (b, m) in parameter space. However, vertical lines can give rise to unbounded values of the parameters m and b. Hence, a different parameter pair, denoted as the polar coordinate, should be used. The straight line and its polar transform are given in Fig. 5.

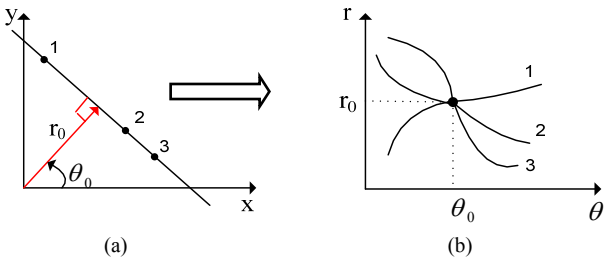

(a) (b)

Figure 5. Hough transform (a) Straight line space (b) Hough space

In Fig. 5, the linear coordinate system is converted to a polar coordinate system. The polar coordinates are represented as

$$r = x\cos(\theta) + y\sin(\theta) \tag{2}$$

where the shortest vector from the origin to the line can be represented by (r, θ) pairs. In the polar coordinate system, a straight line is plotted as a point, as shown in Fig. 5 (b). Many points pass through this point, and each constitutes a different curve in Hough space. The Hough transform is an algorithmic method used to detect the lines in a real image. Each point depicted in Fig. 5 (a) has two common parameters (r, θ). Although each point draws a different curve in Hough space, the intersection point of the set of points is common, as shown in Fig. 5 (b). The intersection points are determined using a voting method. The Hough transform uses an accumulator array for the voting process. The steps of the Hough transform are given in Fig. 6.

```
//E← Binary image
// x← Width of the E
//y← Height of the E
Initialize step
- Canny algorithm is applied to real image to
obtain binary image.
Main steps
for i← 1 to x
    for j← 1 to y
        if (E(i,j) is an edge)
            for θ← 0 to θmax
                r← x*cos(θ)+y*sin(θ)
                r← round (r)
                H(θ,r)← H(θ,r)+1
            end for
        end if
    end for
end for
```

Figure 6. The main steps of Hough transform

After the accumulator matrix H is obtained, a peak location algorithm is applied to detect the largest elements of the matrix. An inverse Hough transform is applied to the peaks to obtain the straight lines in the real image. In this study, the search region of the contact wire is determined by using the Hough transform. Canny edge detector algorithm is applied to each frame of the pantograph video, and then the resulting binary image is obtained. The Hough transform detects the straight lines in the binary image. The upper side of the pantograph is searched for the straight lines found via the Hough transform. However, Hough transform finds all lines in an image and the horizontal line should be searched to obtain the upper side of the pantograph. Fig. 7 illustrates the Hough transform, based on the contact wire's search region determination.

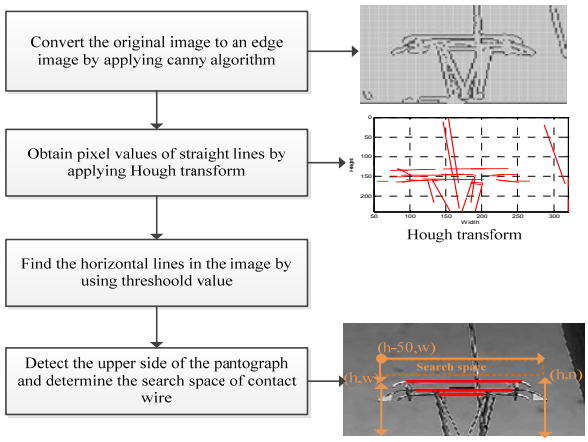

Figure 7. Hough transform based determination of upper bar of pantograph and search space of contact wire

In Fig. 7, because the search space of the contact wire has been limited in the image, a resulting noise effect can be observed as a result of the reduced image quality. Only a small region of the image will be scanned to find the position of the contact wire. The starting point of the search space is selected as 50 pixels above the pantograph bar. The lines of the pantograph upper side, which are founded by the Hough transform, have maximum widths and are generally straight. After the search space has been determined for the current video, the contact position of the overhead wire should be determined and saved in an array. This array will be used to detect the disorder between the contact wire and pantograph. The proposed algorithm is given in Fig. 8.

```
function ypos=contactposition(E,h,w,n)
h,w← Starting pixels of search space
n← End pixel of width of search space
xpos← Position of contact wire

i← h-50;
j← w;
while i<h
  while j<n
    if (E(i, j)==0)
      count← is_contactwire(E,i,j,H);
      if count>threshold
        xpos← [xpos, j];
        i← h;
        j← n;
      else
        j← j+1;
      endif
    endif
    j← j+1;
  endwhile
  i← i+1;
endwhile
```

```
function count=is_contactwire(X,i,j,H)
nn← Number of neighbor pixels
Count← Number of edge pixel in
determined neighborhood

count← 0;
for a=i:h
  for b=j-nn:j+nn
    if X(a, b)==0
      count← count+1;
      break;
    endif
  endfor
endfor
```

Figure 8. Detection of contact wire's position

In Fig. 8, the algorithm takes the edge image of the current frame and finds the position of the contact wire. The algorithm takes the input and output parameters of the search space obtained from the Hough transform. If the algorithm detects a candidate pixel, it uses the is_contactwire method to inspect whether the detected pixel is the contact wire or not. The is_contactwire algorithm searches for the position of the contact wire in the horizontally given neighborhood. The obtained results are compared to a threshold value in the contactposition algorithm. When the position of the contact wire has been found, the algorithm is terminated. The positions of the contact wire is detected and saved to an array for each frame in the video.

B. The Detection of Contact Wire Anomalies

The contact wire position, which is obtained from each frame, is stored as a series. The series of positions gives useful information regarding the condition of the contact wire. The first step in the algorithm is the generation of a symbol sequence from the time series. An entropy-based method has been presented for this purpose. The continuous-domain signals are converted to a discrete domain in this method, and the essential dynamical behavior of the system is maintained [26]. The first step of the method is to separate the continuous signal into partitions.

For a time series, let the variables of N and $|\Sigma|$ show the length of the time series and the size of the alphabet, respectively [27]. The set of symbols is represented by an alphabet $\Sigma=\{\sigma_1, \sigma_2, \sigma_3,...\}$. First, the signal is sorted in ascending order, and then, the signal is partitioned into a data segment of length $\lfloor N/|\Sigma| \rfloor$. Every sample of the signal forms an element of any partition. If a region has rich information in the entropy-based partition, it also will have more symbols, and a finer partition can be achieved in this region. Otherwise, a region with sparse information has fewer symbols, implying a coarser partition. An entropy-based partition reflects the small variations in the signal [28]. When a signal is partitioned, the partition sizes may not all be equal. However, the probabilities of the symbols are equal. The performance of the method is affected by the alphabet size $|\Sigma|$. If this variable is selected to be small, the method will not reflect the characteristic of the signal. However, larger values use more computational resources. A Shannon entropy-based method is used to select the optimal value of the alphabet size. The Shannon entropy is given in (3), as

$$H(k) = -\sum_{i=1}^{k} p_i \log_2 p_i \tag{3}$$

where p_i and k represent the probability of occurrence of a symbol σ_i and the number of symbols, respectively. The number of symbols in the D-Markov machine is determined by using the change in entropy. This change is given by

$$h(k) = H(k) - H(k-1) \ \forall_k \geq 2 \quad (4)$$

An algorithmic approach is used to select the alphabet size. The algorithm is terminated when the h (k) value is smaller than a threshold value ε_h, where $0 < \varepsilon_h < 1$. The algorithm of the alphabet size selection is given in Fig. 9.

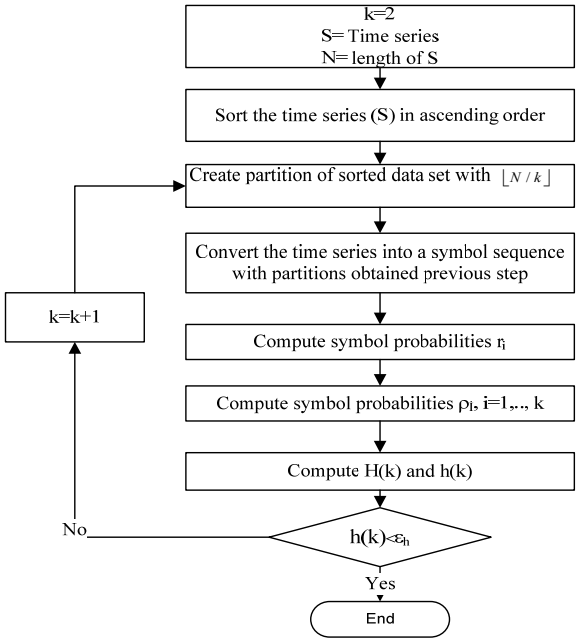

Figure 9. The algorithm of alphabet size selection

In Fig. 9, the threshold value (ε_h) affects the size of the symbol alphabet. When a small threshold value is selected, the numbers of symbols in an alphabet increase. This also increases the noise effect. A large threshold value decreases the number of symbols in an alphabet and the capability of pattern identification is reduced, as well.

After the number of symbols in an alphabet is determined, the finite state machine will be constructed. Each state of the machine is related to a partition. The D-Markov machine is an appropriate method for quantifying the diversity or similarity of two patterns. The D-Markov machine is represented with a state-transition matrix (Π). The sum of each row of the state-transition matrix is equal to one. The number of states in the D-Markov machine is given by $|\Sigma|^D$. The finite state machine moves from one state to another when any event occurs. A signal example and the constructed D-Markov machine are given in Fig. 10.

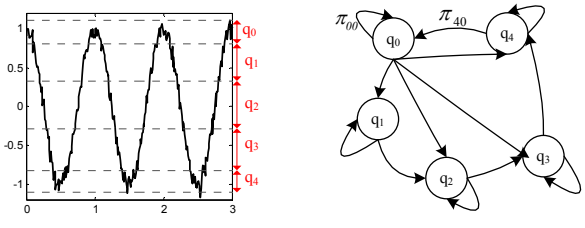

(a) (b)

Figure 10. A signal example and D-Markov machine (a) Signal and states (b) D-Markov machine

In Fig. 10, the alphabet size $|\Sigma|$ is found to be five for a noise-contaminated signal $\cos(2 * \pi * t)$, based on use of the entropy-based algorithm. Probabilities of the state transitions are represented by $\pi_{ij}(\sigma_l)$. In this matrix, the current and transition state are given by i and j, respectively. The symbol q_i is one element of alphabet Σ. While any system is monitored with a state machine, the transitions between different states occur with different frequencies. In a state machine, the number of state transitions and a special symbol from the alphabet are determined. The state probabilities and transition probabilities from one state to another are determined. The transition from any state i to state j ($\pi_{ij}(\sigma_l)$) is calculated as

$$\pi_{ij}(\sigma_l) = n_i^{(\sigma_l)} \Big/ N_i \quad (5)$$

where $n_i^{(\sigma_l)}$ represent the number of times the symbol occurred in state i. The total number of symbols in state i is given by N_i and is calculated as $N_i = \Sigma_k \, n_i^{(\sigma_k)}$.

IV. Experimental Results

Monitoring of the contact wire gives useful information about the quality of collected current. If the wire contacts the same location of the pantograph, the friction increases. This friction produces an arc, causing a loss of the contact between the pantograph and contact wire. The proposed algorithm is applied to a real pantograph's video. The sequences of images are acquired from a camera, mounted on the roof of the locomotive. The video of the pantograph system is saved for a determined time. While the camera captures a frame, the algorithm scans the current frame to find the position of the contact wire. The experimental setup of the proposed algorithm is given in Fig. 11.

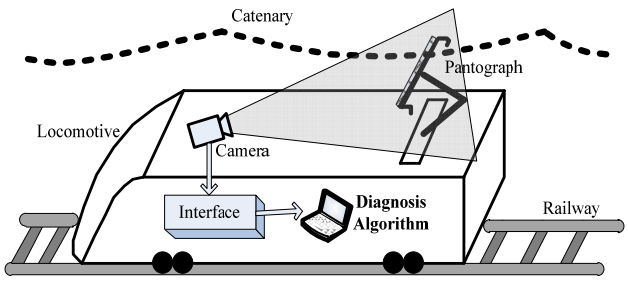

Figure 11. The experimental setup

The algorithm consists of three steps: the first step includes the edge detection from an image via the canny algorithm and reveals the upper side of the pantograph by applying the Hough transform. The second step detects the contact wire position. In the last step, the extracted signal for the contact wire along the video is analyzed using the D-Markov machine, and the anomalies are determined. In each step of the algorithm, one frame is extracted from the video and then is converted to a gray scale image. Each gray scale frame is filtered for noise reduction and sharpness of the objects in the image. The image is then converted to a

binary image, and the canny algorithm is applied to image. The pantograph video without arcing is taken as the healthy condition. An original frame and its edge image are given in Fig. 12 for a healthy condition.

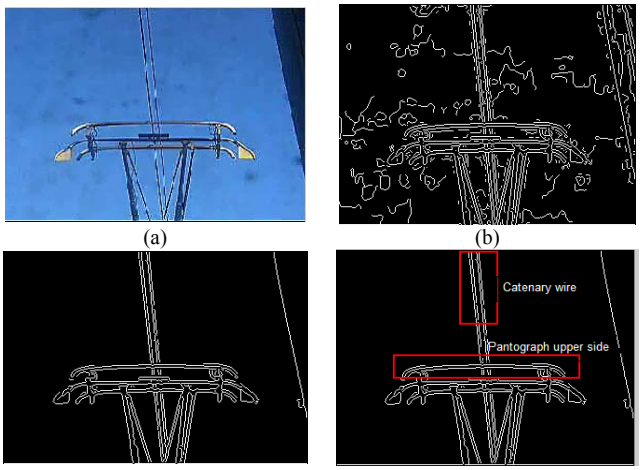

(a) (b) (c) (d)

Figure 12. Canny edge detection algorithm on healthy pantograph image (a)A frame of pantograph video (b)Canny algorithm (c) Canny algorithm with noise reduction (d) Catenary wires and pantograph upper side

In Fig. 12 (a), the sharpened image is depicted, and the canny edge detection method is applied to this image in Fig. 12 (b). When an appropriate filter has been used in the canny algorithm, the noise in the edge image is reduced, as shown in Fig. 12 (c). An appropriate threshold value removes the noises and the shape of the pantograph are revealed. Canny algorithm have low and high thresholds. In this study, the high and low thresholds are selected as 0.2 and 0.08, respectively. After the edge image of the current frame is extracted, the region of analysis should be determined. In Fig. 12 (d), this region is given inside a red rectangular window. The goal of this study is to detect and follow the contact wire in the closest proximity to the pantograph head. Detection of the pantograph upper side plays an important role in obtaining the search region of the contact wire. Hough transform is applied to each frame for obtaining the pantograph head. The pantograph head is not a straight line, but small displacements in the vertical direction are allowed. Appropriate threshold values should be defined for Hough transform. In this study, three parameters are defined. The first parameter specifies the maximum number of peaks to identify. This parameter is selected as 10. The second parameter is a nonnegative scalar value that specifies the threshold at which values of Hough transform matrix are considered to be peaks. The value of this parameter is taken by multiplying the maximum of Hough transform matrix with 0.3. An appropriate value of slope parameter is selected in order to detect horizontal lines. For the upper side line of the pantograph image, the slope value of x-axis is selected as [-5^o, 5^o]. This parameter eliminates the lines that their slopes are higher. Fig. 13 shows the results of Hough transform and threshold defined Hough transform for healthy and faulty conditions.

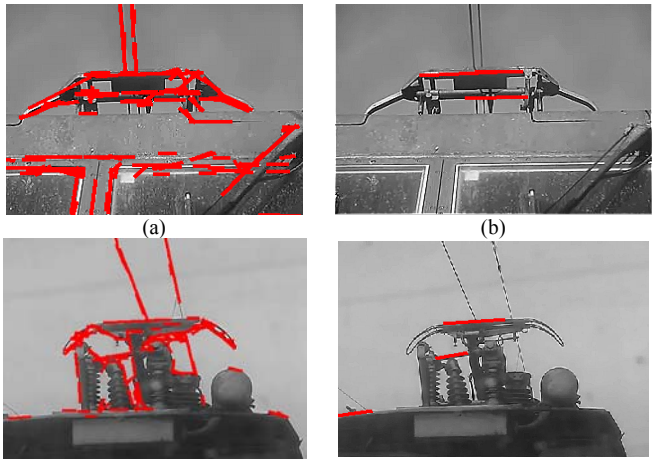

(a) (b) (c) (d)

Figure 13. Pantograph detection by Hough transform for healthy and faulty conditions (a) Hough transform for healthy condition (b) Threshold determined Hough transform for healthy condition (c) Hough transform for faulty condition (d) Threshold determined Hough transform for faulty condition

As shown in Fig. 13, the position of the pantograph head has been correctly determined for each condition. The position of the pantograph does not change further in the vertical direction. The vibrations on the mounted camera may change the viewpoint of the pantograph. The position trajectories of the pantograph head are given in Fig. 14 for healthy condition.

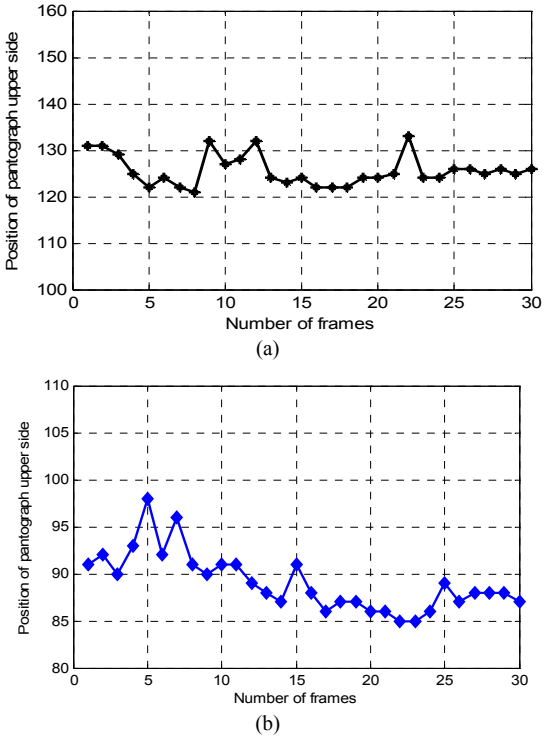

(a) (b)

Figure 14. Position trajectories of pantograph head (a) Healthy condition (b) Faulty condition

After the identification of the pantograph upper side, the next step is devoted to detection of the contact wire. The position of the contact wire is determined by applying the contactposition algorithm to the search region. The threshold value of contactposition algorithm is selected as 30. This threshold value shows minimum number of pixels in the specified neighborhood. The proposed algorithm was applied to four pantograph videos. As a performance index,

successful detection rate of the contact wire is used for each condition. Table I shows the results of detection rate.

TABLE I. ANALYSIS RESULTS FOR EACH CONDITION

Condition	Detection rate of the contact wire	
	Successful	Unsuccessful
Healthy Condition-1	474	10
Healthy Condition-2	508	12
Faulty Condition-1	305	24
Faulty Condition-2	358	19

In Table I, successful rate denotes the number of frames in which the position of the contact wire is detected successfully. When the algorithm cannot detect the contact wire, the unsuccessful detection rate is increased. If an abrupt change has occurred in two adjacent frames, this problem will be solved by replacing them with previous value. The obtained signal is normalized with z-score normalization. This technique centers the original signal at the zero mean and scales it to a unitary standard deviation. This normalization technique is given in (6).

$$pos_{normalized} = \frac{pos - \mu_{pos}}{\sigma_{pos}} \quad (6)$$

In (6), μ_{pos} and σ_{pos} denote the mean and standard deviation, respectively. The contact wire trajectories are given in Fig. 15 for both healthy and faulty conditions, respectively.

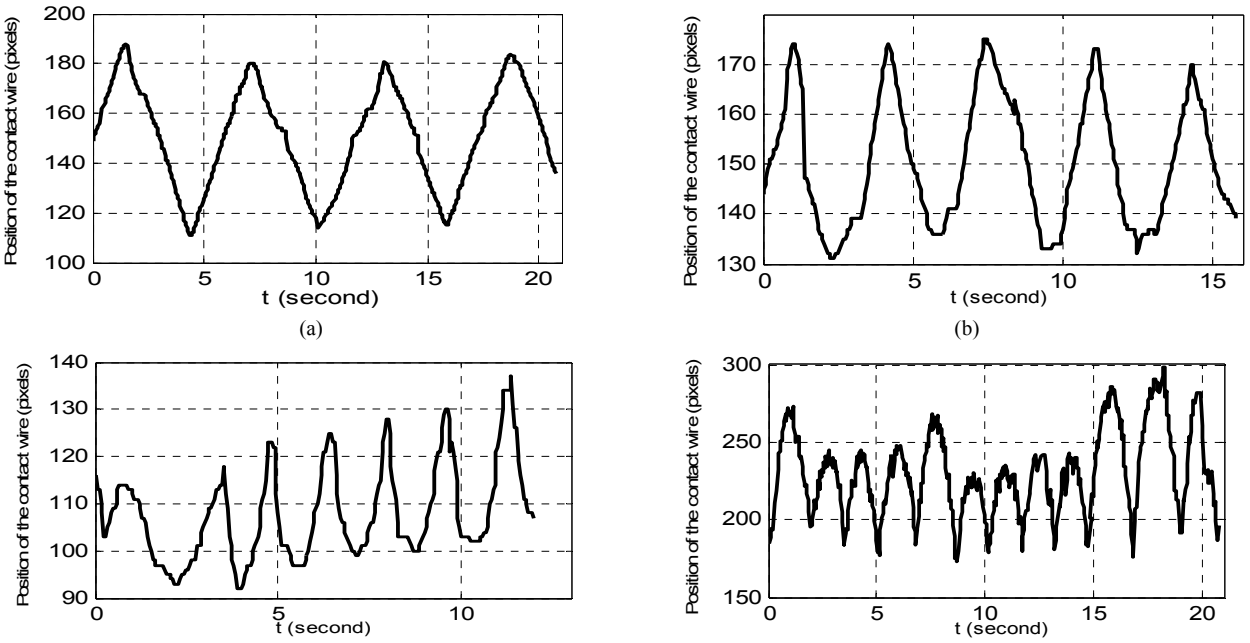

Figure 15. Contact positions for healthy and faulty conditions (a) Contact position for healthy condition-1 (b) Contact position for healthy condition-2 (c) Contact position for faulty condition-1 (d) Contact position for faulty condition-2

As shown in Fig. 15, the contact wire zigzags a balanced motion over the pantograph in a healthy condition. In a faulty condition, the contact wire draws more zigzags in some parts of the pantograph than in others. The more contact occurred on some parts of the pantograph causes arcing between the contact wire and pantograph. The motion of the contact wire possesses a faulty condition disorder. The contact wire draws more zigzags on the bottom of the image than other pixels.

After the zigzag signal of the contact wire has been obtained, the partitioning process converts this data set into a sequence of symbols. This representation simplifies the monitoring process for the catenary wire. The first step in the D-Markov machine is selection of the alphabet size. In this paper, the movement signal of the contact wire is partitioned into segments using entropy partitioning. The results of entropy partitioning and segmentation of the signal are given in Fig. 16.

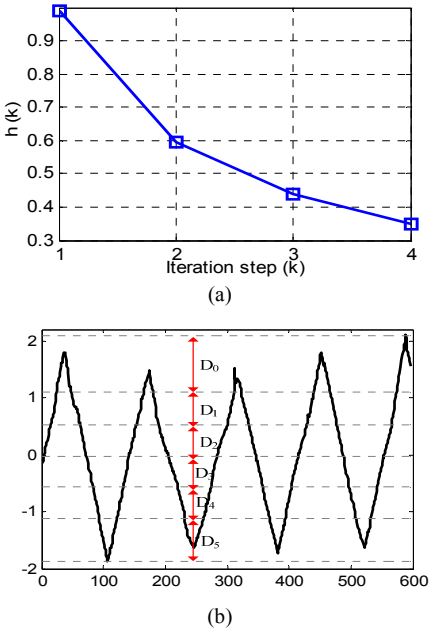

Figure 16. Entropy based discretization and state machine construction of contact wire signal (a) Maximum entropy method (b) Segmentation of signal

In Fig. 16 (a), the maximum and minimum of the series are found, and entropy-based partitioning is applied to the series to split the series into regions. In the algorithm, the threshold value (ε_h) is selected to be 0.3, and when the calculated h (k) value is smaller than this threshold, the alphabet size will be determined. With the selected threshold value, the entropy-based partitioning method finds six states. According to the threshold value, the segmentation of the signal are depicted in Figs. 16 (b). After construction of the D-Markov machine, the state transitional probabilities ($\pi_{ij}(\sigma_l)$) between the states are determined, where i is the source state and j is the target state. Two parameters are counted for each state of the D-Markov machine, including the number of times a state visited and the number of times a symbol occurred. The state probabilities and the state-to-state transition are calculated using these parameters. The first column of the matrix represents the original state, and the first row represents the state following transition. The row sums of these matrices are equal to one. The state transition matrices are given in Table II for two healthy conditions.

TABLE II. STATE TRANSITION MATRIXES FOR HEALTHY CONDITIONS

(a) State transition matrix for healthy condition-1

	D_0	D_1	D_2	D_3	D_4	D_5
D_0	**0.9515**	0.0388	0.0097	0	0	0
D_1	0.0412	**0.9175**	0.0412	0	0	0
D_2	0	0.0385	**0.9135**	0.0481	0	0
D_3	0	0	0.0404	**0.9091**	0.0505	0
D_4	0	0	0	0.0426	**0.9043**	0.0532
D_5	0	0	0	0	0.0404	**0.9596**

(b) State transition matrix for healthy condition-2

	D_0	D_1	D_2	D_3	D_4	D_5
D_0	**0.8824**	0.1176	0	0	0	0
D_1	0.0248	**0.9339**	0.0413	0	0	0
D_2	0	0	**0.9138**	0.0862	0	0
D_3	0	0	0	**0.8750**	0.1250	0
D_4	0	0	0	0.0656	**0.8049**	0.1295
D_5	0	0	0.0152	0	0.0606	**0.9242**

In Table II (a) and (b), although the matrixes have maximum probabilities for the diagonal elements, nonetheless they have minimum probabilities for the other elements. The probability values of the non-diagonal elements of the matrixes increase in a faulty condition. State transition matrixes of two faulty conditions are given in Table III.

TABLE III. STATE TRANSITION MATRIXES FOR FAULTY CONDITIONS

(a) State transition matrix for faulty condition-1

	D_0	D_1	D_2	D_3	D_4	D_5
D_0	**0.6964**	0.1429	0.0893	0	0	0.0714
D_1	0.1194	**0.6567**	0.1642	0.0299	0.0299	0
D_2	0.0286	0.0952	**0.6476**	0.1238	0.0381	0.0667
D_3	0.0233	0.0465	0.2326	**0.4651**	0.1860	0.0465
D_4	0	0.0455	0.0303	0.1212	**0.5909**	0.2121
D_5	0.0377	0	0.1132	0	0.0943	**0.7547**

(b) State transition matrix for faulty condition-2

	D_0	D_1	D_2	D_3	D_4	D_5
D_0	**0.8500**	0.1	0	0	0.05	0
D_1	0.019	**0.9143**	0.0667	0	0	0
D_2	0	0.1429	**0.6905**	0.1667	0	0
D_3	0	0.0213	0.1277	**0.7021**	0.1489	0
D_4	0	0	0.0227	0.1364	**0.3164**	0.5227
D_5	0	0	0	0.0333	0.1333	**0.8333**

In Table III (a), the probabilities of the diagonal elements are decreased. However, the probabilities of the other elements are increased. This condition occurs due to the disorder between the pantograph and contact wire. In Table III (b), the probability values of D_0, D_1, and D_5 are higher than others because the irregularity of the signal are grouped at these points. The proposed method presents a new approach for the monitoring of the pantograph-catenary system. D-Markov-based state machine detects the contact points where more contact with the wire. There is more contact in the states of D_0, D_1, and D_5 than other states. Therefore, wear at these points will be more. There are a few studies in the literature to monitor pantograph-catenary system. The common disadvantage of these studies is that the proposed methods analyze the pantograph in a laboratory environment. The proposed method is compared to these studies in order to show the efficiency of the proposed method. Table IV gives the accuracy rate and the average time of each method.

TABLE IV. THE LOCATION OF THIS STUDY IN THE LITERATURE

Paper	**Used method**	**Accuracy rate (%)**	**Average Time (ms)**
[1]	Segmentation and morphological image processing	82.59±10.91	360.00
[6]	Wavelet analysis of current and voltage signals	78.55±6.15	117.19
[12]	Image segmentation and geometric transform	76.5±9.19	57.50
[14]	Analysis of contact point by Hough transform	75.4±5.20	200.00
This study	**Edge detection, Hough transform, and D-markov based state machine**	**95.82±2.47**	**67.50**

In Table IV, the accuracy rate and average time of each algorithm is compared in order to show the efficiency of the proposed method. The average processing time of each frame is calculated in milliseconds. The performance criteria of image processing methods is determined by the detection rate of pantograph or contact wire in each frame. In [1] and [12], the performance measure was selected as the rate of correctly detection of the pantograph in each frame. The images of pantograph carbon strips were analyzed for in-service monitoring of wear and damage on pantograph [1]. Thickness of pantograph strip is used to detect the pantograph defects. When a fault is at an inception stage, the method may fails to detect the faults. A geometric structure and image segmentation based method was proposed to detect pantograph in an image [12]. The occurrence of arc and healthy condition are discriminated by using wavelet analysis in [6]. However, this method is affected from pantograph type because a new geometric model should be created for each pantograph type. Pantograph overhead contact wire was analyzed by using thermal images [14]. The temperature along the strip was analyzed and occurred arcs were detected. It is obviously indicated that the detection rate of the proposed method is higher than other methods. The proposed method in this paper brings many advantages to the literature. It is suitable for real-time analysis. Contact point is by detecting the pantograph height. Contact wire is monitored throughout the video and, and the resulting irregularities are detected with D-Markov state machine. Unlike other methods in TABLE IV, the contact related problems are detected by tracking the position of contact wire. D-Markov based state machine

determines the position of more contact between pantograph and contact wire. This information can be used for the detection of wear points of a pantograph.

V. CONCLUSIONS

This paper presents a new approach for monitoring the catenary-pantograph system. Canny edge detection was selected for image edge detection to deal with the image edge of the pantograph slipper. The experimental results of the proposed method showed that the position detection of the contact wire was an efficient method for detecting arc faults and disorder in the contact between the pantograph and contact wire. In the literature, the use of image processing-based conditions to monitor pantograph systems only had been performed in the laboratory environment. However, the proposed method can be applied in real-time. Realization of the proposed method is not only low cost, but also, this technique can be setup for a real system. The results show that the proposed algorithm can be used as an online technique, suitable for real-time detection of the disorders in contact between the pantograph and catenary system. When this system is correctly installed, reliably operation of high-speed electrified railways will be ensured.

Monitoring of the contact wire and the active pantograph control system brings the following contributions, listed as

- The development of a railway measurement and inspection train for both conventional and high-speed railway lines,
- Real time fault diagnosis with high accuracy and immunity to environmental conditions,
- A low cost measurement system, and
- Increasing the safety and comfort levels of railway systems.

REFERENCES

[1] L. G. C. Hamey, T. Watkins, S. W. T. Yen, "Pancam: In-service Inspection of Locomotive Pantographs," In: IEEE Conference on Digital Image Computing Techniques and Applications, Los Alamitos, 2007, pp. 493-499. http://dx.doi.org/10.1109/DICTA.2007.4426837.

[2] C. ODonnell, R. Palacin, J. Rosinski, "Pantograph Damage and Wear Monitoring System,", In: IEEE Conference on Railway Condition Monitoring, London, England, 2006, pp. 178-181.

[3] S. Midya, D. Bormann, T. Schütte, R. Thottappillil, "Pantograph Arcing in Electric Railways—Mechanism and Influence of Various Parameters—Part II: With AC Traction Power Supply," IEEE Trans. on Power Delivery, 2009, pp. 1940–1950. http://dx.doi.org/10.1109/TPWRD.2009.2021036.

[4] W. Zhang, N. Zhou, R. Li, G. Mei, D. Song, "Pantograph and Catenary System with Double Pantographs for High-Speed Trains at 350 Km/H or Higher," Journal of Modern Transportation, vol. 19, pp. 7-11, Mar. 2011. http://dx.doi.org/10.1007/BF03325734

[5] P. M. Keen, "Monitoring Overhead Line Equipment," In: IEE Current Collections for High Speed Trains Seminar, London, England, 1998, pp. 3/1-3/3. http://dx.doi.org/10.1049/ic:19981002.

[6] S. Barmada, M. Tucci, "Use of Advanced Signal processing Techniques for Arcing Detection on AC Pantograph Catenary Systems," In: Proc. of Pantograph Catenary Interaction Framework for Intelligent Control, Amiens, France, 2011, pp. 1-7.

[7] A. Pisano, E. Usai, "Contact Force Regulation in Wire-Actuated Pantographs via Variable Structure Control," In: 46th IEEE Conference on Decision and Control, LA, USA, 2007, pp.1986-1992. http://dx.doi.org/10.1109/CDC.2007.4434183.

[8] S. Barmada, M. Raugi, M. Tucci, F. Romano, Arc detection in pantograph-catenary systems by the use of support vector machines-based classification", IET Electr. Syst. Transp., doi: 10.1049/iet-est.2013.0003, to be published.

[9] P. Boffi, G. Cattaneo, L. Amoriello, A. Barberis, G. Bucca, M. F. Bocciolone, A. Collina, and M. Martinelli, "Optical Fiber Sensors to Measure Collector Performance in the Pantograph-Catenary Interaction," IEEE Trans. on Sensors, 2009, pp. 635-640. http://dx.doi.org/10.1109/JSEN.2009.2020244.

[10] R. Uwe, R. Schneider, "Automated optical inspection of overhead contact line systems," Siemens Efficient Railway Solutions, 2010.

[11] O. Bruno, A. Landi, M. Papi, L .Sani, "Phototube sensor for monitoring the quality of current collection on overhead electric railways," Proc. Instn Mech. Engrs, Part F: J. Rail and Rapid Transit, vol. 215, pp. 231-241, 2001. http://dx.doi.org/10.1243/0954409011531549

[12] A. A. Boguslavskii, S. M. Sokolov, "Detecting Objects in Images in Real-Time Computer Vision Systems Using Structured Geometric Models," Journal of Programming and Software, vol. 32, pp. 177-187, May-June 2006. http://dx.doi.org/10.1134/S036176880603008X

[13] S. Midya, D. Bormann, T. Schütte, and R. Thottappillil, "Pantograph Arcing in Electrified Railways—Mechanism and Influence of Various Parameters—Part I: With DC Traction Power Supply," IEEE Trans. On Power Delivery, 2009, pp. 1931-1939. http://dx.doi.org/10.1109/TPWRD.2009.2021036.

[14] A. Landi, L. Menconi, L. Sani, "Hough Transform and Thermo-Vision for Monitoring Pantograph–Catenary System," Proceedings of the Institution of Mechanical Engineers Part F: Journal of Rail and Rapid Transit, vol. 220, pp. 435-447, July 2006. http://dx.doi.org/10.1243/0954409JRRT41

[15] S. Östlund, A. Gustafsson, L. Buhrkall, M. Skoglund, "Condition Monitoring of Pantograph Contact Strip," In: 4th IET IEEE International Conference on Railway Condition Monitoring, Derby, England, 2008, pp. 1–6.

[16] M. Li, W. Z. Yong, G. X. Rong, W. Li, Y. Kai, "Edge Detection on Pantograph Slide Image," In: 2nd IEEE International Congress on Image and Signal Processing, Tianjin, China, 2009, pp. 1-3. http://dx.doi.org/10.1109/CISP.2009.5304714.

[17] Z. X. Heng, G. X. Rong, W. Z. Yong,W. Li, Y. Kai, "Study on the Edge Detection and Extraction Algorithm in the Pantograph Slipper's Abrasion," In: IEEE International Conference on Computational and Information Sciences, Chengdu, China, 2010, pp. 474-477. http://dx.doi.org/10.1109/ICCIS.2010.123.

[18] T. Koyama, "A Method to Measure the Contact Force of Pantographs through Image Processing," Railway Technology Avalanche, vol. 37, pp. 219, 2011.

[19] P. V. Verschraegen, "A Model of the Pantograph Arc Impedance for 50 Hz Catenary Voltage," Master of Science Thesis, Stockholm, Sweden, 2010.

[20] I. Aydin, M. Karakose, and E. Akin, "A New Contactless Fault Diagnosis Approach for Pantograph-Catenary System," In: 15th IEEE International Conference On Mechatronika, Prague, Czech Republic, 2012, pp. 1-6.

[21] S. Midya, "Conducted and Radiated Electromagnetic Interference in Modern Electric Railways with Emphasis on Pantograph Arcing," PhD Thesis, Kungliga Tekniska Höghskolan, Stockholm, Sweeden, 2009.

[22] R. C. Gonzalez, R. E. Woods, "Digital Image Processing," Prentice Hall; 3 edition, pp. 976, 2007.

[23] J. Canny, "A Computational Approach to Edge Detection," IEEE Trans. Pattern Analysis and Machine Intelligence, 1986, pp. 679-698. http://dx.doi.org/10.1109/TPAMI.1986.4767851.

[24] S. Oprisescu, E. Barth, "3D Hand Gesture Recognition using the Hough Transform", Advances in Electrical and Computer Engineering vol. 13, pp. 71-76, http://dx.doi.or/10.4316/AECE.2013.03012.

[25] X. Ning, Y. Wang, "Object extraction from architecture scenes through 3d local scanned data analysis", Advances in Electrical and Computer Engineering, vol. 12, pp. 73-78, http://dx.doi.org/10.4316/AECE.2012.03011.

[26] V. Rajagopalan, A. Ray, R. Samsi, J. Mayer, "Pattern Identification in Dynamical Systems via Symbolic Time Series Analysis," Pattern Recognition, vol. 40, pp. 2897-2907, Nov. 2007. http://dx.doi.org/10.1016/j.patcog.2007.03.007

[27] R. Samsi, A. Ray, J. Mayer, "Early Detection of Stator Voltage Imbalance in three-phase Induction Motors," Electric Power Systems Research, 2005, pp. 478-483. http://dx.doi.org/10.1109/ACC.2005.1469981.

[28] I. Aydin, M. Karakose, E. Akin, "A new method for early fault detection and diagnosis of broken rotor bars," Energy Conversion and Management, vol. 52, pp. 1790-1799, April 2011. http://dx.doi.org/10.1016/j.enconman.2010.11.018.